APPLIED RESEARCH

Enhanced Wide Spectrum Photocatalytic Activity by in-Situ Magnetite-Graphite Nanoplatelets Heterostructure

S. A. L. SAMEERA[1]**, N. P. EDIRISINGHE**[1,2]**, YASUN Y. KANNANGARA**[1]**,**
SHADEEPA KARUNARATHNE[1,3]**, K. R. KOSWATTAGE**[4]**, H. C. S. PERERA**[5]**,**
G. DAS[5]**, M. M. M. G. P. G. MANTILAKA**[4,6]**, AND W. P. S. L. WIJESINGHE**[1]

[1]Sri Lanka Institute of Nanotechnology (SLINTEC), Pitipana, Homagama 10200, Sri Lanka
[2]Research and Innovation Division, Ministry of Education, Battaramulla, Sri Lanka
[3]Department of Design and Engineering, Bournemouth University, BH12 5BB Poole, U.K.
[4]Centre for Nanodevices Fabrication and Characterization (CNFC), Faculty of Technology, Sabaragamuwa University of Sri Lanka, Belihuloya 70140, Sri Lanka
[5]Department of Physics, Khalifa University, Abu Dhabi, United Arab Emirates
[6]Institute of Materials Engineering and Technopreneurships (IMETechno), Kandy 20000, Sri Lanka

Corresponding authors: W. P. S. L. Wijesinghe (slwijesinghe@gmail.com) and G. Das (gobind.das@ku.ac.ae)

ABSTRACT A UV, visible and NIR range irradiation responsive magnetite/graphite nanoplatelets composite was successfully synthesised via a single-step facile in-situ electrochemical exfoliation method using natural vein graphite. The spectral analysis revealed that as-synthesised photocatalyst could rapidly degrade the organic dyes with 96.1, 78.0 and 82.6 % efficiency in 120 minutes under respective UV, Visible, and NIR ranges of the electromagnetic spectrum. The formation of the magnetite-graphite nanoplatelet (GNP) nanocomposite was verified with X-ray diffraction (XRD), Fourier transform infrared absorption spectroscopy (FTIR), Raman spectroscopy, X-ray photoelectron spectroscopy (XPS), scanning electron microscopy (SEM), transmission electron microscopy (TEM), and atomic force microscopy (AFM) analysis. The scaffold of highly electrically conductive GNP helps magnetite nanoparticles for the efficient distribution of photoinduced electrons generated by the photocatalytic activity to participate in the photodegradation of organic dyes, through rapid superoxide radical formation. The current work presents a hypothesized mechanism for the photocatalyst composite synthesis, while a thorough discussion was made on the improvements in photocatalytic degradation kinetics under multiple irradiation conditions through the synergy of the magnetite and GNP. High efficiency, low-cost facile synthesis, easy up scalability, and the easy removal of the catalyst as needed via an external magnetic field can be identified as major benefits of as-synthesised green catalyst, which can be readily used in dye pollutant removal and wastewater treatment applications.

INDEX TERMS Magnetite graphite nanoplatelets, electrochemical synthesis, photocatalysis, dye pollutants, wastewater treatment.

I. INTRODUCTION

Semiconductor metal oxide nanoparticles have been used in many applications in solar energy harvesting, electronics,

The associate editor coordinating the review of this manuscript and approving it for publication was Santosh Kumar.

optics, electrochemical, etc. [1]. The application of semiconductor metal oxide nanoparticles as a photocatalyst is one of the significant areas in solar energy harvesting. It is capable of modifying the photoreaction while absorbing light from the surrounding. However, there are common drawbacks when semiconductor metal oxide nanoparticles

act as photocatalysts, such as low conductivity and high recombination of photogenerated electrons, which reduces the catalytic efficiency [2], [3]. Graphene related materials are widely used to overcome the problems in semiconductor metal oxide nanoparticles as the superior electrical conductivity in graphene is beneficial to have an enhanced the electron-accepting and transporting properties of the composite. Therefore, when semiconductor metal oxide nanoparticles are hybridised with graphene into nanocomposites, it increases the removal of photogenerated electrons from the semiconductor surfaces via the $\pi-\pi$ electron interactions while reducing the electron recombination processes in the semiconductor materials [4]. In addition, aggregation due to the Van der Waals interaction between the graphene layers can also be prevented with the composite formation of graphene and metal oxide nanoparticles as the metal oxide nanoparticles occupy the space in between the layers, increasing the composite materials' surface area. As a result, the photocatalytic effect of the graphene-based semiconductor metal oxide nanocomposites has been improved [4].

Furthermore, iron oxide (IO) is one of the widely used visible light active photocatalysts in solar energy harvesting applications [5], [6]. Fe_3O_4 and maghemite(γ-Fe_2O_3) are magnetic materials because of their ferromagnetic properties [7]. Fe_3O_4 contains oxide forms of both Fe^{2+} and Fe^{3+} ions ($FeO.Fe_2O_3$) and can be both an n-type and p-type semiconductor with a 2.5 eV band gap [8]. Because of the fast electron sharing of both iron species, the electrical resistivity of Fe_3O_4 is lower than other iron oxides; therefore, it is considered a half-metal [8]. Also, the Fenton reaction and Haber–Weiss reaction cycles are more prominent in Fe_3O_4; therefore, hydroxyl radical generation is faster in Fe_3O_4-based photocatalysts than in other IO nanoparticles [9], [10]. Therefore, photocatalytic effect of the iron oxide nanoparticles has successfully been used to degrade organic contaminants in wastewater [11].

Graphene and its derivatives are widely used supporting materials to enhance the magnetic IO nanoparticles' adsorption capacity and photocatalytic activity. For instance, as graphene oxide (GO) and reduced graphene oxide (rGO) are graphene derivatives used to prepare IO/GO and IO/rGO nanocomposites, respective. adsorption capacities of organic and inorganic water pollutants of both IO/GO and IO/rGO nanocomposites were reported to be higher than that of the IO nanoparticles [12], [13]. Among other IO nanoparticles, Fe_3O_4 has the fastest photocatalytic activity and, Fe_3O_4 has widely been combined with graphene and its derivatives to synthesise nanocomposites for practical applications. Even though Fe_3O_4 NPs/ GO composite can significantly increase the photocatalytic activity [14], [15], the activity will not sustain as the GO flakes in the nanocomposite are subject to further oxidisation due to the degradation of GO under the Photo-Fenton reaction [16]. To overcome this GO decomposition in Fe_3O_4/GO nanocomposite, rGO has been employed instead of GO as a less oxidative graphene derivative which helps to delocalise excited electrons through the conductive

graphene layer since rGO is a conductive material. Therefore, electron delocalisation decreases with the oxidation level of the graphene. This can be easily understood by analysing the variation of magnetisation of the Fe_3O_4 nanoparticles. Magnetization is significantly reduced with the conductivity of the graphene derivatives in the nanocomposite because it allows delocalisation of the 3d electron via charge transfer from iron to graphene [17]. For instance, literature mentioned that the magnetic dispersibility of Fe_3O_4 with rGO is higher than disperse of Fe_3O_4 with GO [18].

As discussed above, many efforts have already been attempted to develop a synthetic route for the fabrication of rGO/ Fe_3O_4 instead of GO/Fe_3O_4 to acquire superior photocatalytic activity and excessive fabrication yield. Some of the examined routes are the hydrothermal /solvothermal method, deposition via electrochemical and electrophoresis processes, chemical electrolysis deposition, and deposition *via* physical contact and mixing [4], [19], [20]. Each synthesis method has its own advantages and limitations [4], [19], [20]. However, limited studies have been carried out for the photocatalytic nanocomposites of Fe_3O_4 and graphene/ graphite nanoplatelets electrochemically exfoliated or physically exfoliated. One-step electrochemical exfoliation employed in this work has the novelty of functionalizing graphite nanoplatelets (GNP) from natural vein graphite and simultaneously combining them with Fe_3O_4 nanoparticles to produce magnetically active GNP (MGNP) nanocomposite using hazardous-free chemicals, whereas most of the previous studies required two-step processes and/or harsh chemicals.

Further, the as-synthesized MGNP catalyst has exhibited wide-band photocatalytic activity in the different domains of the solar spectrum against UV, Visible, and NIR radiations over the magnetite catalyst indicating its superiority over GNP. Especially the degradation of methylene blue (MB) by 82.6% in 120 minutes under NIR is one of the very impressive findings during the study. In addition, a hypothesized mechanism is also introduced on the synthesis route of the novel MGNP catalyst. The ability to remove the catalyst from a solution after treatment easily is also beneficial for its practical use. Furthermore, the method involves the use of natural resources, hazardous-free chemicals, and a cost-effective eco-friendly synthesis approach, which could motivate its scalability and commercial viability as well as sustainable value-addition to natural resources.

II. EXPERIMENT
A. ELECTROCHEMICAL SYNTHESIS OF MGNP
A mixture of 0.002 moles of Fe^{2+} and 0.004 moles of Fe^{3+} ions was mixed in 100 ml of deionised water. The anode electrodes made from Sri Lankan vein graphite and cathode electrodes made from stainless steel (SS) were immersed in the prepared 350 mL of 5 M Na_2SO_4 solution. The distance between the anode and cathode was around 4 cm and remained constant throughout the electrochemical process. To expand the graphite layers, 2 V were applied for

30 minutes through two electrodes. After 30 minutes, the potential was increased to 10 V to begin the exfoliation. In parallel, 100 mL of Fe^{2+}/Fe^{3+} ions mixture was added dropwise to the Na_2SO_4 solution for 4 h to the reaction mixture. After that, it was stirred continuously for 12 h to complete the synthesis of magnetic graphene. Thereafter, the obtained black colour in the reaction mixture was collected and washed several times with deionised water via a vacuum filter. After MGNP was dried in a vacuum oven, it was used to characterise and test its photocatalytic activity. The whole experiment was repeated for the control setup without adding the Fe^{2+}/Fe^{3+} ion mixture and obtained GNP to compare with the synthesised MGNP.

B. CHARACTERIZATION OF THE SYNTHESISED MATERIAL
A crystallographical study was carried out by X-ray diffraction (XRD) (model: Bruker D4 X-ray scattering system with Ni-filtered Cu Kα radiation) in the range of 15 – 75°. Raman spectra were recorded from 500 to 3500 cm^{-1} on Senterra Bruker Raman Microprobe using a 532 nm, 10 mW laser and 100X objective lens to determine the quality of the graphene structure in MGNP and GNP. Then functional groups in the synthesised MGNP and GNP were analysed by Fourier Transform Infrared (FTIR) Spectroscopy with the Bruker Vertex80 in the range of 500 – 4000 cm^{-1} of wavenumber in ATR mode. External topologies and internal morphologies of the synthesised materials were identified by transmission electron microscopy (TEM) (model: Jeol 2100 microscope), and scanning electron microscopy (SEM) model: (Hitachi SU6600 microscope), respectively. Additionally, atomic force microscopy (AFM) (model: The Park Systems XE 100 instrument) was used to estimate the surface roughness, and to investigate the thickness of the MGNP nanocomposites as well. The XPS measurements were obtained using a Scienta ESCA 200 spectrometer in an ultrahigh vacuum with a base pressure of 10^{-10} mbar to investigate the bond formation and to calculate the band gap of the MGNP nanocomposite. Thermo gravimetric analysis (TGA) was performed to examine the variation of composite mass with the temperatures.

C. INVESTIGATION OF PHOTOCATALYTIC ACTIVITY
The methylene blue (MB) and reactive yellow dyes (RYD) were used as model dyes to evaluate the photocatalytic degradation of the synthesised MGNP nanocomposites. 4 mg of each of the MGNP catalysts were dispersed in 50 mL of each of the 20 ppm dye aqueous solutions, separately. The catalyst suspensions were stirred for 5 min under dark conditions, and the photocatalytic tests were carried out separately at room temperature under UV (using 254 nm UV lamp), Visible, and NIR (up to 900 nm) radiation conditions. The distance between the lamp and the base of the beaker was kept at 25 cm. Each experiment was conducted for 120 minutes with 3 mL sample aliquots taken out to analyse dye concentration. At the end of the time intervals dispersed catalysts were magnetically separated by using an external magnet from the

exposed samples and sample was filtered before analysing under UV-visible spectroscopy. All the experiments were triplicated to produce concise results. Similar experiments were conducted under dark conditions to investigate the dye adsorption effect of the synthesised nanoparticles. The dye degradation efficiency of the catalyst was calculated using (1) given below [21].

$$q_e = \frac{C_0 - C_e}{C_0} \times 100\% \qquad (1)$$

where q_e is the efficiency of dye degradation, C_0 is the initial concentration, and C_e is the concentration of dye after irradiation by light.

III. RESULTS AND DISCUSSION
A. FORMATION OF GNP AND MGNP
The electrolysis of water is the cause of the exfoliation of graphite into GNP during the synthesis process. Water molecules split into hydrogen and oxygen gases at the cathode and anode, respectively, when the applied electrical potential is greater than the standard electrolysis potential (i.e. 1.5 V) of the water [22]. These essential reactions are shown in the schematic representation of the experimental setup in Figure 1a. The figure depicts the cathodic reaction, which produces oxygen, and the negatively charged stainless steel (SS) cathode, which produces hydrogen gas bubbles and hydroxyl ions with the applied voltage of 2.0 V for 30 min. Due to the continuous electric field, these hydroxyl ions are attracted to positively charged graphite anodes and are trapped between interlayers in the graphite anode and oxidised while producing gaseous oxygen (O_2). As a result of this O_2 evolution, the graphite's interlayer distance increases. However, it is difficult to obtain rapid exfoliation in water to obtain GNP while breaking the expanded sheets into small pieces because of the low electrical conductivity of the water. Therefore, some acids and salts have been used as electrolytes to improve the electrical conductivity of the reaction medium *via* better electron transformation. This increases the oxygen evolution rate at the anode.

Additionally, anions in the electrolyte, such as sulfate anions, fluoride anions, and metal halides, intercalate to the positively charged graphite anode and enhance the layer expansion. In addition to aqueous electrolyte solutions of inorganic acids and salts, sulfate-ion-based electrolytes such as H_2SO_4, $(NH_4)_2SO_4$, Na_2SO_4, and K_2SO_4 have also been widely used because SO_4^{2-} ions act as a catalyst to enhance the evolution of oxygen at the positively charged electrode. According to reaction (2), intercalated SO_4^{2-} ions can be oxidised into $S_2O_8^{2-}$ at the anode. However, in an aqueous medium, SO_4^{2-} oxidation reaction (02) is blocked by oxidising water into O_2 (reaction 3) because the standard redox potential of SO_4^{2-} (+2.01 V) is higher than the standard redox potential of water (+1.5 V).

Reaction 4 shows the oxidation of SO_4^{2-} ion to SO_4^{-} ion, and the produced SO_4^{-} ions oxidise water molecules (see reaction 5) by generating O_2 gas quickly at the anode, while
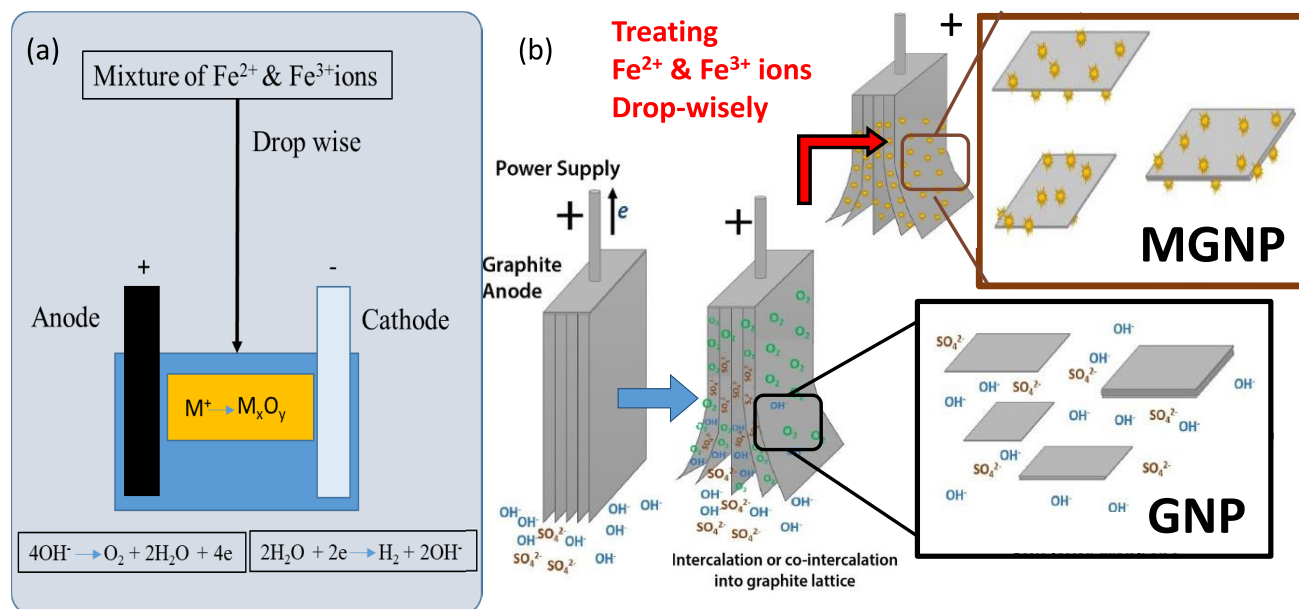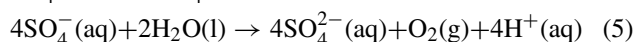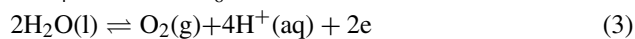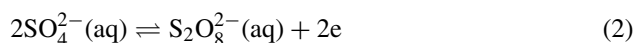
FIGURE 1. Schematic representation of (a) the experimental setup and reactions involved in the synthesis of MGNP and (b) Schematic overview of anodic exfoliation and functionalization mechanisms of GNP and MGNP.
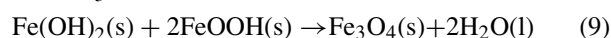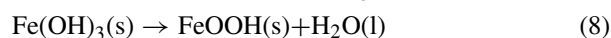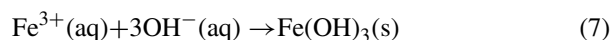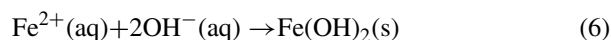
the oxidised SO_4^{2-} ions are reproduced as catalysts in the medium. Because of this rapid oxygen generation at the graphite anode, SO_4^{2-} based electrolytes are more efficiently exfoliated graphite into graphene.

$$2SO_4^{2-}(aq) \rightleftharpoons S_2O_8^{2-}(aq) + 2e \quad (2)$$

$$2H_2O(l) \rightleftharpoons O_2(g) + 4H^+(aq) + 2e \quad (3)$$

$$SO_4^{2-}(aq) \rightarrow SO_4^{-}(aq) + e \quad (4)$$

$$4SO_4^{-}(aq) + 2H_2O(l) \rightarrow 4SO_4^{2-}(aq) + O_2(g) + 4H^+(aq) \quad (5)$$

As explained above, the rapid exfoliation of graphite starts with applying 10 V due to the rapid evolution of O_2 gas between layers of graphene. This study provides a novel one-step method to produce magnetic graphene composites. While a 10 V constant potential is applied, a mixer of Fe^{2+} and Fe^{3+} ions is added slowly. These positive ions get chemically bind to exfoliated layers of graphene flakes through the functional groups present in the exfoliated graphene flakes. Then OH^- ions produced at the cathode react with bonded Fe^{2+} and Fe^{3+} ions, releasing graphene flakes when travelling to the anode. After the reaction between Fe^{2+} and Fe^{3+} ions and OH^- ions, iron hydroxides of Fe^{2+} and Fe^{3+} iron species are deposited on the graphene flakes. The chemical reactions for these reactions are shown as reactions (6 and 7). Finally, deposited iron hydroxides on graphene flakes react with each other and convert them into magnetite nanoparticles according to the reactions (8 and 9) and reaction medium conditions.

The schematic diagrams shown in Figure 1 clearly illustrate the experimental setup and functionalisation mechanism of MGNP synthesis. The formation of Fe_3O_4 as magnetic

nanoparticles on the exfoliating graphene flakes is described in the material characterisation section. The photocatalytic activity of the synthesised composites is discussed under the dye degradation results in the Section.

$$Fe^{2+}(aq) + 2OH^-(aq) \rightarrow Fe(OH)_2(s) \quad (6)$$

$$Fe^{3+}(aq) + 3OH^-(aq) \rightarrow Fe(OH)_3(s) \quad (7)$$

$$Fe(OH)_3(s) \rightarrow FeOOH(s) + H_2O(l) \quad (8)$$

$$Fe(OH)_2(s) + 2FeOOH(s) \rightarrow Fe_3O_4(s) + 2H_2O(l) \quad (9)$$

B. XRD CHARACTERISATION OF MATERIALS

XRD patterns of produced Fe_3O_4, MGNP, and GNP are given in Figure 2a. The XRD pattern in Figure 2a agrees with the Fe_3O_4 standard peak positions of JCPDS card no. 19-0629. Various peaks of the Fe_3O_4 sample are observed at 2θ values of 18.3°, 30.1°, 35.2°, 43.1, 53.6°, 56.9°, and 62.5° due to miller index reflections of (111), (220), (311), (400), (422), (511) and (440), respectively. Also, the XRD pattern given in Figure 2a agrees with the GNP standard peak positions of the standard XRD pattern of Graphite (JCPDS card no. 41-1487) [23]. The XRD peaks of the GNP sample are found at 2θ values of 26.1°, 44.4° and 54.3° which are due to the reflection from the basal planes of (002), (100), and (004), respectively, which is identical in JCPDS card, file no. 41-1487. This indicates that the GNP has a similar crystal pattern to the raw Graphite. Figure 2a shows the XRD pattern of the prepared MGNP sample. The presence of XRD peaks in MGNP at relevant positions of both Fe_3O_4 and GNP confirms the formation of MGNP nanocomposite. In XRD patterns of MGNP, the peak found at $\sim$26.1° is attributed to the (002) basal plane of MGNP, and the peaks
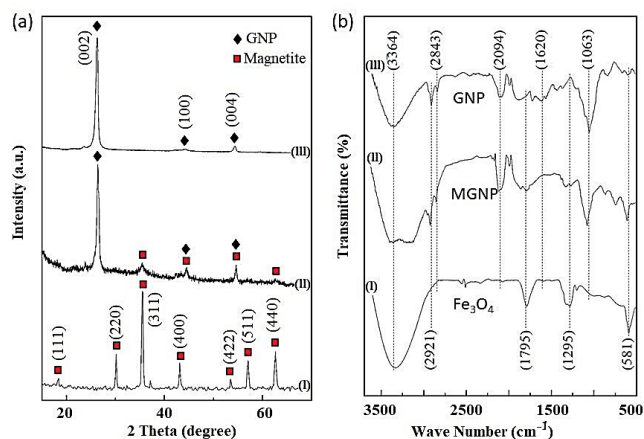
FIGURE 2. XRD patterns (a) and FTIR spectra (b) of Fe3O4, MGNP, and GNP.

found at 35.2° and 62.5° are attributed to the (311) and (440) basal planes, respectively. Also, the peaks found at 44.4°, and 54.5° are formed due to the overlap of peaks generated from both Fe_3O_4 and GNP. Similar XRD patterns have been reported for Fe_3O_4 and GNP nanocomposites, confirming the composite's XRD pattern [24]. Also, similar XRD patterns of graphene (rGO, GO, expanded graphite, etc.)- Fe_3O_4 have been commonly obtained and published elsewhere [23], [25], [26], [27]. Since maghemite (c-Fe_2O_3) with an inverse spinel structure has lattice parameters similar to magnetite, it is difficult to differentiate it only by XRD results [28]. FTIR was used to clarify the existing lattice structure.

C. FTIR CHARACTERISATION OF MATERIALS

The FTIR spectra of Fe_3O_4, MGNP, and GNP are shown in Figure 2b. Various vibrational bands have been observed throughout the experimental spectral range from 500 – 3700 cm^{-1}. The peak at 580 cm^{-1} is attributed to the stretching vibration mode associated with the metal-oxygen Fe–O bonds in the crystalline lattice of Fe_3O_4 [29], which is different from that of maghemite (630 cm^{-1}) [30]. This absorption band at 580 cm^{-1} of Fe_3O_4 still exists in Fe_3O_4 and MGNP, respectively. Moreover, there are many oxygen contained functional groups in GNP, such as C=O (carbonyl) at 1730 cm^{-1} [31]; C=C (aromatics) at 1621 cm^{-1} [22]; C-O (carboxy) at 1403 cm^{-1}; C-O (epoxy) at 1227 1295 cm^{-1} [32]; and C=O (alkoxy) at 1061 cm^{-1} [31]. It should be noted that the alkoxy, epoxy, and carboxyl functional groups are almost entirely removed in MGNP, implying that MGNP is a composite made of Fe_3O_4 and Graphite nanoplatelets (GNPs). The C-H stretching band at around 3000 cm^{-1} [32] is shown both for GNP and MGNP with a slight shift to 2921 cm^{-1}, indicating that, even when magnetite nanoparticles were deposited on the GNP surface, the graphite structure remained exposed. The stretching bands in 1795 cm^{-1} and 3425 cm^{-1} are attributed to OH-bending and OH-stretching vibrations, respectively.

D. RAMAN SPECTROSCOPIC EVALUATION OF THE MATERIALS

The prepared GNP and MGNP were characterized and compared with pure graphite's Raman spectra, as shown in Figure 3, which helps study disorders and defects in the crystal structure. It is often employed to characterize graphite and its derivatives. The Raman spectra of graphite show a strong G peak at 1570 cm^{-1} due to the first-order scattering of E2g mode [33]. GNP and MGNP show their G peak shifted slightly towards 1585 cm^{-1} due to the attached functional groups of the graphite surface. As explained in the experiment, these functional groups are oxygenated and formed when electrochemical exfoliation occurs.

The disorders, which are determined by the intensity ratios of D and G bands in Figure 3, explained GNP has a higher ratio compared to the MGNP, suggesting a decrease in the average size of the sp^2 domains upon the exfoliated GNP and can be explained by graphitic domains are combined with oxygen-rich functional groups more in GNP because of the MGNP reduced on the cathode in electrochemical exfoliation [34].
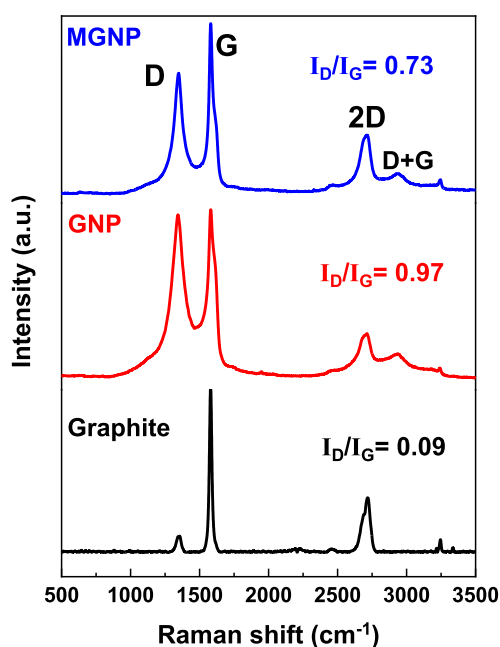

FIGURE 3. Raman spectroscopy of graphite, GNP and MGNP.

E. XPS STUDIES OF MATERIALS

The full XPS survey spectrum in Figure 4(a) shows the presence of Fe, C, and O in the range between 0- 1300 eV. The C 1s spectrum in Figure 4(b) displays the sp^2 hybridized carbon peak at 284.1 eV, indicating the aromatic ring of the remaining GNP structure [22].

Because of electro-exfoliation, the functional groups are bound to the surface of the carbon skeleton of the GNP. The GNP surface has shown C-OH and C-O-C peaks at 285.5 eV and 286.5 eV, respectively. The Fe-O bond at 530.6 eV and the O-H bond at 531.9 eV indicate the magnetite

particle nature and activated groups in the graphite structure of the MGNP [35]. In addition, the O 1s spectrum shows a C-O-C ether peak at 533.3 eV in Figure 4(c), is agreed with the corresponding C-O-C ether peak at 286.5 eV in the C 1s spectrum in Figure 4(b) [36]. This indicates the functional groups that appeared on the graphite surface at electro-exfoliation of the MGNP. The 725.0 eV and 711.4 eV peaks can be attributed to Fe $2p_{1/2}$ and $2p_{3/2}$, respectively [36]. The Fe $2p_{3/2}$ could be divided into two peaks at binding energies of 713.7 eV and 711.3 eV, indicating the bonding of Fe^{2+} and $Fe^{3+,}$ each with oxygen (Figure 4d), respectively [36]. The satellite peaks of Fe $2P_{1/2}$ and Fe $2P_{3/2}$ can be observed around 733.4 eV and 719 eV, respectively [37]. A slight shift of the peaks to the higher binding energy occurred for the Fe 2p spectrum (deviation of 0.8 eV). This shift is due to the bonding of Fe^{2+}/ Fe^{3+} with O or other functional groups, which may form during electro-exfoliation [38].
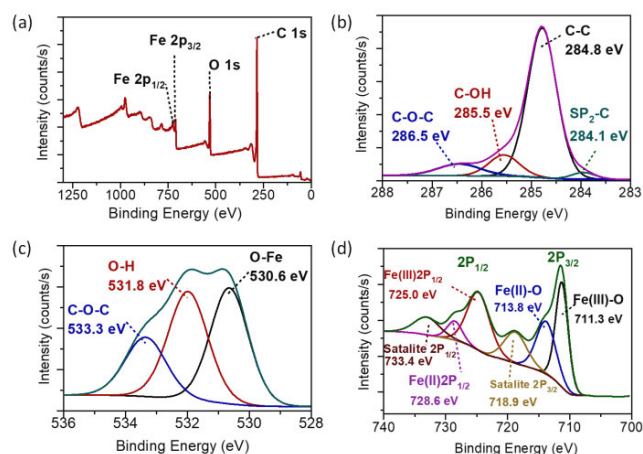

FIGURE 4. Raman XPS survey and high-resolution spectra of MGNP; (a) survey spectrum, (b) C 1s, (c) O 1s, and (d) Fe 2p.

F. ELECTRON MICROSCOPE STUDIES

Figure 5(a) shows SEM micrographs of the GNP nanostructures and Figure S2 shows TEM images of GNP, clearly depicting the exfoliated layers. As Figure 5(a) exhibited, the graphite layers remained without broken pieces, although the exfoliation separates the layers. Figure 5(b) exhibited the heterogeneous surfaces of the MGNP, which confirmed the Fe_3O_4 nanoparticles sediment on the GNP surface. Thus, photocatalytic nanoparticles were exhibited in Fig. 6(c) and 6(d). The graphite clusters were broken around 800 nm-sized pieces (Figure 5(c)), and 200 nm-sized particle clusters (Figure 5(d)) were dispersed on the GNP surface. This will enhance the photocatalytic activity due to the GNP surface acting as a platform for exchanging electrons.

The Fe_3O_4 nanoparticle average size is around 10 nm, and clusters of size between 20-50 nm were formed due to magnetic agglomeration (Figure 5(d)). It can be concluded that the Fe_3O_4 nanoparticles emit the electrons under
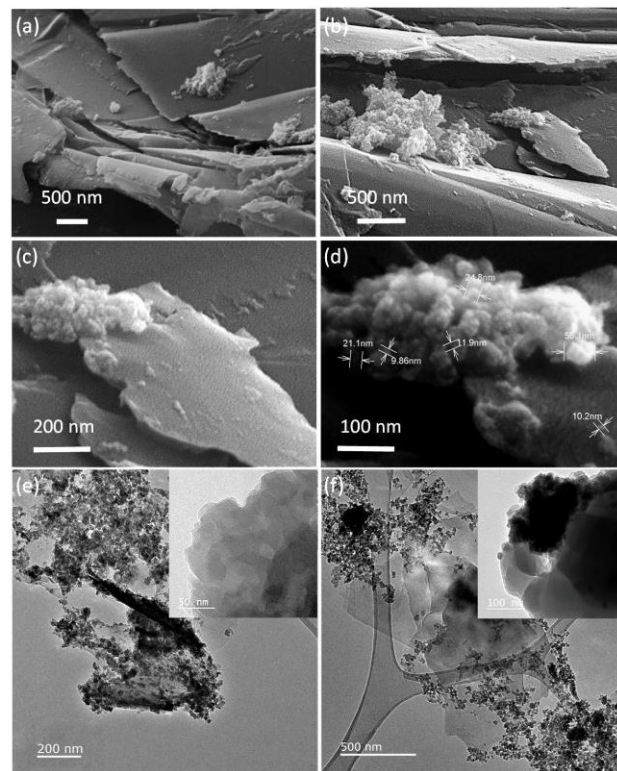

FIGURE 5. SEM images of (a) electrochemically exfoliated GNP and (b – d) MGNP and TEM images (e, f) of MGNP composite particles.

photocatalytic activities, and the GNP surfaces collect those electrons to produce radicals. The TEM images clearly indicate the multilayered structures of the MGNP nanocomposite (Figure 5 (e-f) and Figure S1). The inset image in Figure 5(e) shows the exfoliated nature of the GNP domains in MGNP. The inset image in Figure 5(f) exhibited Fe_3O_4 and GNP domains, indicating the MGNP nanocomposite's heterogeneous nature.

G. AFM CHARACTERIZATION OF MATERIAL

Figure 6 shows the atomic force microscopy (AFM) images of MGNP nanoparticles carried out in non-contact mode for a 3.0 μm×3.0 μm sized area to investigate the topography and phase distribution. The topography figure (Figure 6(a)) illustrates the two components distributed in different height profiles, coded according to their intensity in color. The light regions have the highest points representing the coagulated Fe_3O_4 particles, and the dark region describes the GNP domains. Phase imaging in Figure 6(b) provides complementary information to the topography image, revealing the variations in the surface properties of the MGNP [20]. It clearly demonstrates the heterogeneous nature of GNP and Fe_3O_4 nanoparticles on the GNP surface. The two-line profiles in Figure 6(b) show the MGNP particles are spread around 250 nm and thicken approximately 70- 90 nm. This finding was further supported by the phase investigated in Figure 5(d) that contrasts two types of domains: lighted

Fe$_3$O$_4$ particles were coated on a dark-colored GNP surface. Figure 6(c) evidenced the particle nature of Fe$_3$O$_4$ on the surface by illustrating the sharp peaks in the phase-3D image.
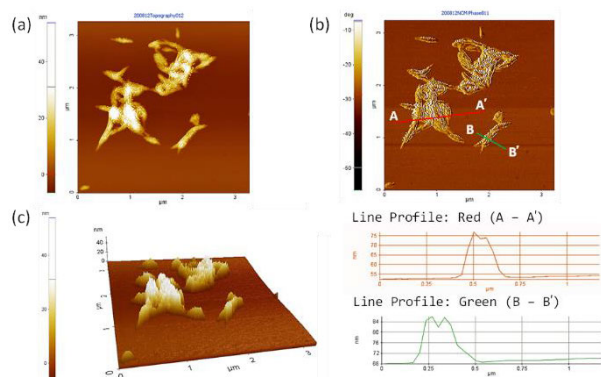

FIGURE 6. Atomic force microscopy images of MGNP (a) topography image, (b) Phase image with the line profiles of the particle surface, and (c) Topographical-3D image.

H. EVALUATION OF MAGNETIC PROPERTIES OF THE MGNP CATALYST

The synthesized heterogeneous structure of MGNP was well characterized as a composite of graphite nanoplatelets (GNP), and magnetite (Fe$_3$O$_4$) during the previous sections. Since the magnetism of the structure is only used at maneuvering of the photocatalyst and for the removal of it from the solution after the treatment, an in-depth analysis on magnetic properties of the material was not conducted. The magnetic nature of the structure was proven by exposing the aqueous solution of the catalyst to an external magnetic field. The image in Figure S10 is clearly indicating that MGNP is very sensitive at the applied external magnetic field, and the video 01 in supplementary is also clear demonstration of the easy maneuver of the MGNP catalyst, and essentially the video illustrates the removal of catalyst from the system upon the treatment.

I. EVALUATION OF PHOTOCATALYTIC PERFORMANCE OF THE MATERIAL

Graphite based materials have shown high adsorbing capabilities [39]. Because of that reason, the kinetic measurements were carried out in dark and light conditions to contrast the photocatalytic degradation from the adsorption. Since the catalysts do not have any energy to stimulate them without photons, photocatalytic degradation cannot occur in dark conditions [21]. Adsorption spectra for MB and RYD are shown in Figures 7(a-b). The adsorption of MB and RYD by the Fe$_3$O$_4$ nanoparticles was very low compared to that of GNP and MGNP due to the high natural adsorption of graphite-based particles. According to Figures 7(a-b), MGNP has higher adsorption than GNP, which can be explained by the improved porosity in MGNP than GNP by a combination of GNP and Fe$_3$O$_4$ nanoparticle. In Figure S3 to S8, the initial stage (T$_0$) did not show any photocatalytic degradation or adsorption before the measurement started. The linear

fitting of the kinetic models of MB and RYD are also shown in Figure 7c and 7d.

The degradation data were fitted by the pseudo-first-order kinetics. The first-order rate constant, K, can be determined by $In(C/C_0) = -Kt$ at a low initial pollutant concentration [40]. Herein, C$_0$ is the initial MB (Figure 7c) and RYD (Figure 7d) concentrations corresponding to the absorbance recorded in irradiation time T$_0$ (0 min.) spectrums in Figure S3 to S8, respectively, while C is the concentration after irradiation time of t. The adsorption rate constant (K) of MB were 4×10^{-4} min^{-1}, 9×10^{-4} min^{-1} and 1.8×10^{-3} min^{-1} for Fe$_3$O$_4$, GNP and MGNP, respectively, as listed in Table 1. The adsorption rate constants (K) of RYD for Fe$_3$O$_4$, GNP and MGNP were 3×10^{-4} min^{-1}, 6×10^{-4} min^{-1} and 1.7×10^{-3} min^{-1}, respectively. GNP and MGNP, having graphene contained compounds, show higher adsorption kinetics with respect to the Fe$_3$O$_4$ due to the highly porous morphology of the GNP and MGNP (see SEM images (Figure 5a and 5b)). In addition, a large surface area could provide more active sites of GNP platforms for the adsorption of MB and RYD, causing increased rate constants of MGNP.

Furthermore, the absorbance spectrums of MGNP and Fe$_3$O$_4$ under visible light conditions were depicted in Figures 8(a-b), respectively. The corresponding degradation rate constant and degradation efficiency were explained in Figures 8c and 8d. After adsorption measurements under dark conditions, the photocatalytic degradation rate constant (K) of MB for Fe$_3$O$_4$ and MGNP were 3.9×10^{-3} min^{-1} and 1×10^{-2} min^{-1}, respectively, as depicted in Table 1. GNP does not exhibit any photocatalytic degradation. The first order rate constant (K) shows the RYD degradation of MGNP was twice larger than the degradation kinetics of pristine Fe$_3$O$_4$. These results indicate that the graphene moieties from GNP exchange the electrons into the superoxide radicals (O$_2^-$) effectively, enhancing the visible light photocatalytic degradation.

To further identify the photocatalytic activity, the photocatalytic performances of the samples were evaluated by the degradation of methylene blue (MB) under visible light, UV and NIR irradiation conditions (Figure 9). Notably after visible light being exposed for 120 min, the degradation efficiency of MB by the pristine Fe$_3$O$_4$ was 49 % and by MGNP was 78 % as shown in Figure 9a. This indicates that the MGNP has higher photocatalytic efficiency in comparison to its pristine Fe$_3$O$_4$ state because GNP moieties are efficiently collecting the charges and distributing them into radical formation reactions. The corresponding UV spectra of photocatalytic degradation of MB are shown in Figures S9-S11.

The corresponding pseudo-first-order kinetic plots are shown in Figure 9b. The photocatalytic degradation rate constant (K) of MB in visible light for Fe$_3$O$_4$ and MGNP were 6.1×10^{-3} min^{-1} and 1.33×10^{-2} min^{-1}, respectively, and are listed in Table 1. Under UV irradiation, both pristine Fe$_3$O$_4$ and MGNP have shown high degradation efficiencies of around 96 % (Figure 9c) and correspond to
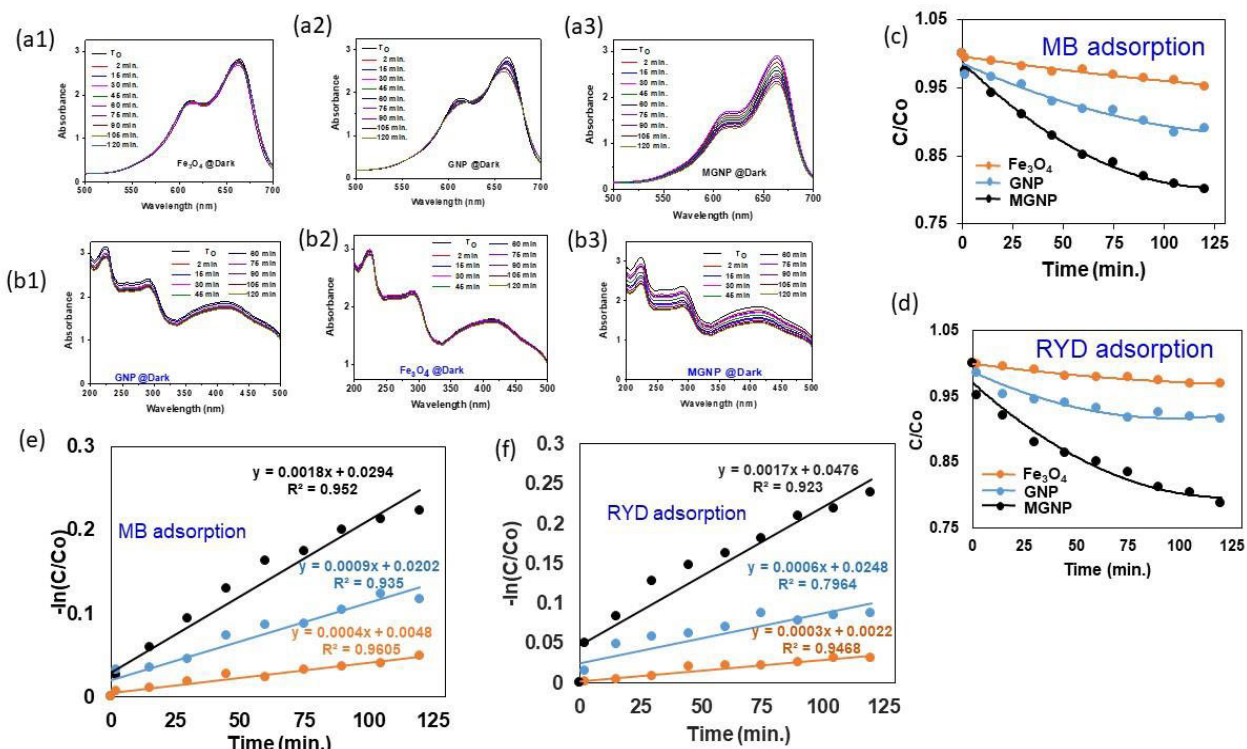
FIGURE 7. Adsorption of (a1-a3) MB and (b1-b3) RYD by the MGNP, GNP and Fe3O4 nanoparticles under dark conditions, corresponding C/C0 vs time curves for (c) MB and (d) RYD, and −ln(C/C0) vs time curves of (e) MB and (f) RYD by the MGNP, GNP and Fe3O4 nanoparticles.

TABLE 1. Degradation kinetics of Photocatalytic materials investigated in the present study.

Sample	Activity	Irradiation Condition	MB		RYD	
			K (min^{-1})	R^2	K (min^{-1})	R^2
Fe_3O_4	Adsorption	Dark	4×10^{-4}	0.9567	3×10^{-4}	0.9468
GNP	Adsorption	Dark	9×10^{-4}	0.935	6×10^{-4}	0.7964
MGNP	Adsorption	Dark	1.8×10^{-3}	0.952	1.7×10^{-3}	0.923
Fe_3O_4	Photodeg.	Visible	6.1×10^{-3}	0.9814	3.9×10^{-3}	0.985
MGNP	Photodeg.	Visible	1.33×10^{-2}	0.9917	1×10^{-2}	0.9787
Fe_3O_4	Photodeg.	UV	2.54×10^{-2}	0.9952	na	na
MGNP	Photodeg.	UV	2.18×10^{-2}	0.9901	na	na
Fe_3O_4	Photodeg.	IR	3.1×10^{-3}	0.9967	na	na
MGNP	Photodeg.	IR	1.31×10^{-2}	0.9864	na	na

(na-not applied; photodeg- photodegradation)

that high kinetic rate constants of 2.54×10^{-2} min^{-1} and 2.18×10^{-2} min^{-1} (Figure 9d), respectively. The photon energy of UV- rays (240 nm) is beyond the threshold value for stimulating the electron-hole pair generation in MGNP and Fe_3O_4 is the reason behind achieving high photocatalytic degradation efficiency and a high first order rate constant (K). In the NIR range (900 nm), the Fe_3O_4 and MGNP samples were exposed to infrared rays for around 120 min. The C/C_0

conversion plots for MB degradation (Figure 9e) obviously showed 32.4 % and 82.6 % of degradation efficiencies for Fe_3O_4 and MGNP, respectively. The corresponding rate constant for MGNP is also very high, 1.31×10^{-2} min^{-1}, which is almost four times of rate constant 3.1×10^{-3} min^{-1} of Fe_3O_4 particles (Figure 9f).

Based on the presented experimental results, it is evident that the photocatalytic activity of MGNP was able to rapidly
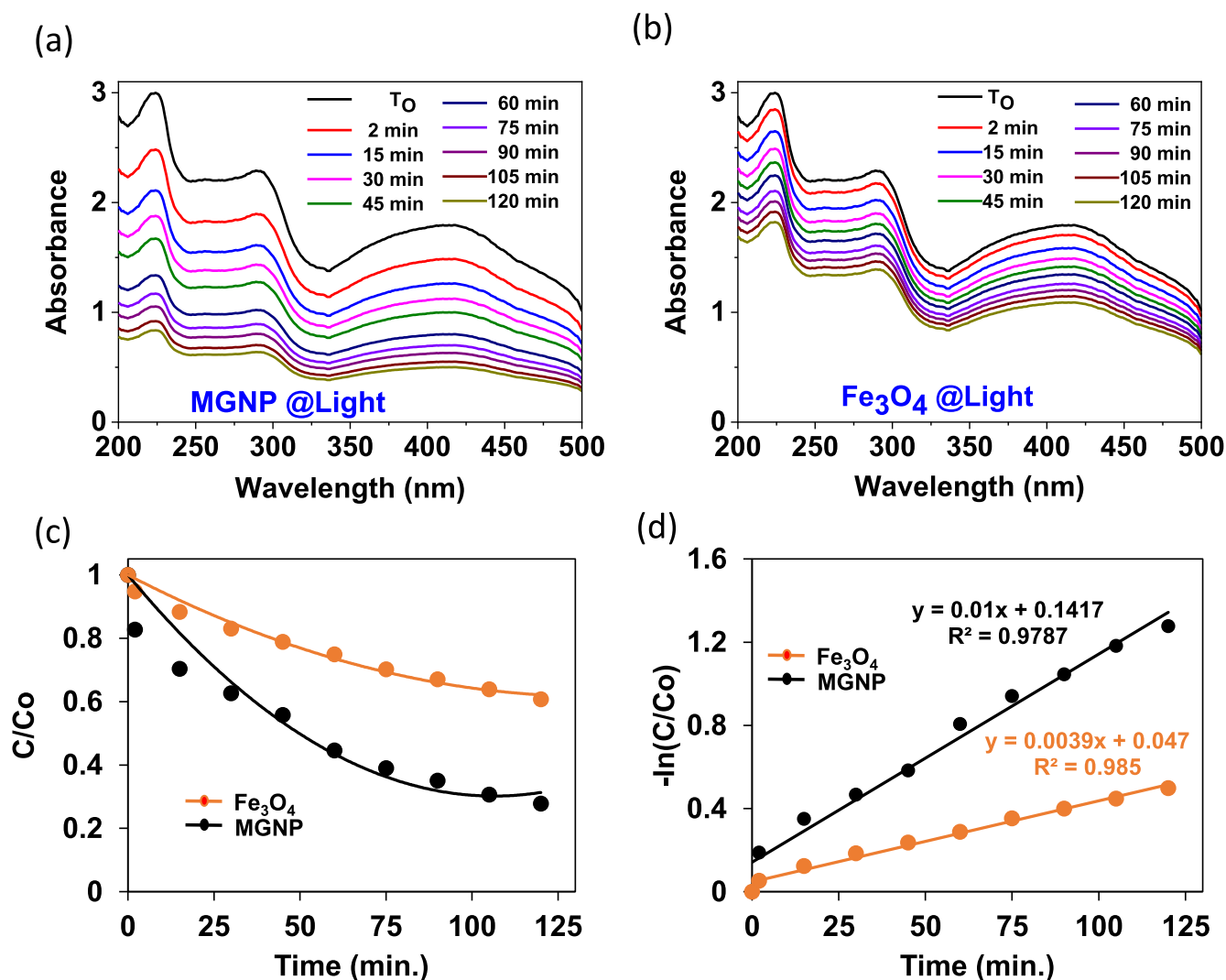
FIGURE 8. Absorbance spectrum of RYD by the (a) MGNP and (b) pristine Fe3O4 under visible light conditions, and (c) C/C0 conversion plots and (d) −ln(C/C0) vs time curves of degradation kinetics of both MGNP and Fe3O4.

decompose organic dyes under UV, visible and NIR irradiation compared to that of pristine Fe_3O_4. We believe that the MGNP is capable of rapid removal of organic dyes due to the following reasons:

- MGNP's GNP moieties adsorb the organic dye molecules;
- GNP can act as a platform to efficiently collect the photogenerated electrons of MGNP nanocomposite particles, reducing the recombination.

Table 1 below summarizes the degradation rate constant for Fe_3O_4, GNP and MGNP under different conditions.

The current work has achieved a degradation efficiency of 78% under visible light, 96.1% under UV light, and 82.6% under NIR by only using a little amount of catalyst (0.08 g/L). There are reported works on graphite/graphene-related materials showing good catalytic properties, hence the rapid removal of dye from the aqueous solution (refer Table S1). Even though higher degradation efficiency has

been achieved in previous studies, it required longer reaction time [14], [41], catalytic reaction performed under UV light [42], adsorption [41] or higher catalytic dosage [14], [41], [43], [44], [45]. It is important to compare our work with graphite-related nanocomposites, which have Fe^{2+}/Fe^{3+} compounds that are beneficial. But most of such systems speed up the degradation via photo-Fenton reaction [14], [42], [45], [46]. It should be noted that in our system, we have not utilized the photo-Fenton reaction, and we were able to achieve 78% degradation efficiency under visible light, whereas other reported works have lower efficiency without the photo-Fenton effect. Besides that, there are, however fewer studies reported on GNP based nanocomposite for NIR responsivity. It is noteworthy that our nanocomposite shows 82.6% of degradation efficiency under NIR illumination. To the author's knowledge, there were not many reports on wide-spectrum sensitive photocatalytic nanocomposites based on graphite-based nanocomposites.
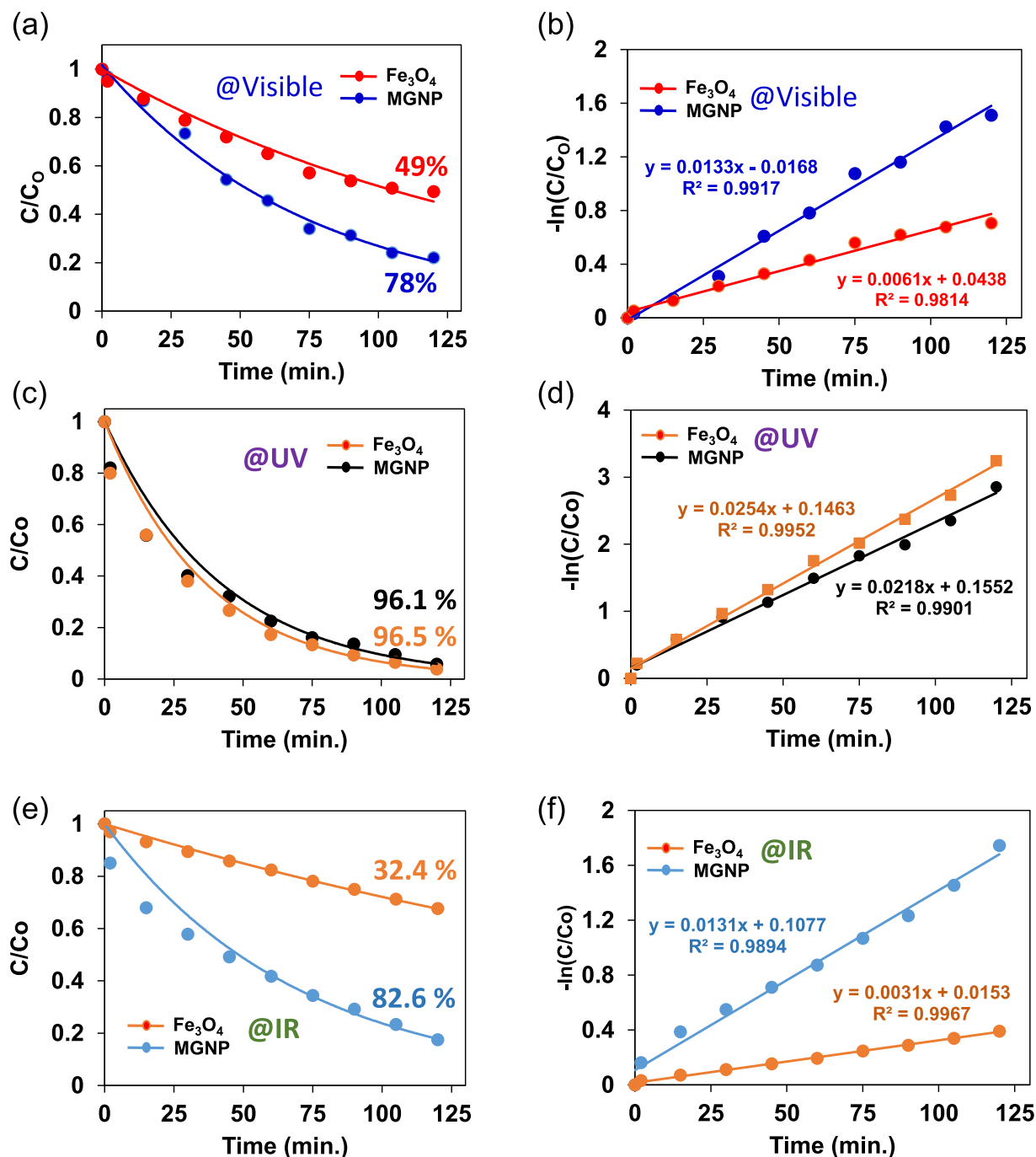
FIGURE 9. Kinetics of photocatalytic degradation of MB dye using MGNP and pristine Fe3O4 under different irradiations. C/C0 conversion plots of MB photodegradation under (a) Visible, (c) UV and (e) IR irradiation, and −ln(C/C0) vs time curves of MB photodegradation under (b) Visible, (d) UV and (f) NIR irradiation.

This research is focusing on modifying naturally available vein graphite material to act as a photocatalyst which is capable of degrading dye under wide-spectrum light as well as easy removal of the catalyst from the aqueous medium.

IV. CONCLUSION

GNP and MGNP-based photocatalysts have been successfully synthesised by the electro-exfoliation technique. MGNP has been formed by electrochemical exfoliation due to the presence of ferrous and ferric ions in the media, and it attracted towards the negatively charged oxygen functionalities formed at the periphery of graphite sheets as the exfoliation been taken place. The RAMAN, XPS, FTIR, SEM, TEM and AFM studies verified the successful formation of the MGNP (magnetite-Graphite Nanoplatelet) composite. The MGNP shows superior photocatalytic activity under UV, visible, and NIR radiations with respective efficiencies of 96.1, 78.0 and 82.6 %, compare to its pristine Fe_3O_4,

which only decompose MB with 96.5, 49, 32.4% respective efficiencies under similar conditions. MGNP showed significant absorbance reduction under IR radiation, indicating upconverted nature. However, Fe_3O_4 and MGNP show expected MB degradation under visible light and UV irradiation. Hence, Methylene blue and Reactive Yellow industrial dyes have been successfully degraded by MGNP material, confirming the industrial significance in MGNP photocatalyst, which could use at the degradation of organic dye wastes in effluents in range of light conditions. In addition, its green and cost-effective synthesis pathway and the ability to guide by and external magnetic field also can be identified as further advantages in the as-synthesised wide spectrum photocatalytic material.

APPENDIX A
Supplementary information.

DECLARATION OF COMPETING INTEREST
The authors declare no conflict of interest, financial or otherwise.

REFERENCES
[1] G. Oskam, "Metal oxide nanoparticles: Synthesis, characterization and application," *J. Sol.-Gel Sci. Technol.*, vol. 37, no. 3, pp. 161–164, Mar. 2006.

[2] A. Jana, E. Scheer, and S. Polarz, "Synthesis of graphene–transition metal oxide hybrid nanoparticles and their application in various fields," *Beilstein J. Nanotechnol.*, vol. 8, pp. 688–714, Mar. 2017.

[3] P. T. Yin, S. Shah, M. Chhowalla, and K.-B. Lee, "Design, synthesis, and characterization of graphene–nanoparticle hybrid materials for bioapplications," *Chem. Rev.*, vol. 115, no. 7, pp. 2483–2531, Apr. 2015.

[4] M. Long, Y. Qin, C. Chen, X. Guo, B. Tan, and W. Cai, "Origin of visible light photoactivity of reduced graphene oxide/TiO2 by in situ hydrothermal growth of undergrown TiO2 with graphene oxide," *J. Phys. Chem. A*, vol. 117, no. 32, pp. 16734–16741, Aug. 2013.

[5] P. Xu, G. M. Zeng, D. L. Huang, C. L. Feng, S. Hu, M. H. Zhao, C. Lai, Z. Wei, C. Huang, G. X. Xie, and Z. F. Liu, "Use of iron oxide nanomaterials in wastewater treatment: A review," *Sci. Total Environ.*, vol. 424, pp. 1–10, May 2012.

[6] P. Saharan, G. R. Chaudhary, S. K. Mehta, and A. Umar, "Removal of water contaminants by iron oxide nanomaterials," *J. Nanosci. Nanotechnol.*, vol. 14, no. 1, pp. 627–643, Jan. 2014.

[7] A. S. Teja and P.-Y. Koh, "Synthesis, properties, and applications of magnetic iron oxide nanoparticles," *Prog. Cryst. Growth Characterization Mater.*, vol. 55, pp. 22–45, Mar./Jun. 2009.

[8] S.-N. Sun, C. Wei, Z.-Z. Zhu, Y.-L. Hou, S. S. Venkatraman, and Z.-C. Xu, "Magnetic iron oxide nanoparticles: Synthesis and surface coating techniques for biomedical applications," *Chin. Phys. B*, vol. 23, no. 3, Mar. 2014, Art. no. 037503.

[9] J. P. Kehrer, "The Haber–Weiss reaction and mechanisms of toxicity," *Toxicology*, vol. 149, no. 1, pp. 43–50, Aug. 2000.

[10] P. Gupta, A. Lakes, and T. Dziubla, "A free radical primer," in *Oxidative Stress and Biomaterials*. Cambridge, U.K.: Academic, 2016, ch. 1.

[11] S. M. Mousa, N. S. Ammar, and H. A. Ibrahim, "Removal of lead ions using hydroxyapatite nano-material prepared from phosphogypsum waste," *J. Saudi Chem. Soc.*, vol. 20, no. 3, pp. 357–365, May 2016.

[12] P. Mishra, S. Patnaik, and K. Parida, "An overview of recent progress on noble metal modified magnetic Fe_3O_4 for photocatalytic pollutant degradation and H_2 evolution," *Catal. Sci. Technol.*, vol. 9, no. 4, pp. 916–941, 2019.

[13] T. Qi, C. Huang, S. Yan, X.-J. Li, and S.-Y. Pan, "Synthesis, characterization and adsorption properties of magnetite/reduced graphene oxide nanocomposites," *Talanta*, vol. 144, pp. 1116–1124, Nov. 2015.

[14] N. A. Zubir, C. Yacou, J. Motuzas, X. Zhang, and J. C. D. da Costa, "Structural and functional investigation of graphene oxide–Fe_3O_4 nanocomposites for the heterogeneous fenton-like reaction," *Sci. Rep.*, vol. 4, no. 1, pp. 1–8, Apr. 2014.

[15] A. Arshad, J. Iqbal, and Q. Mansoor, "Graphene/Fe_3O_4 nanocomposite: Solar light driven Fenton like reaction for decontamination of water and inhibition of bacterial growth," *Appl. Surf. Sci.*, vol. 474, pp. 57–65, Apr. 2019.

[16] Z. Wang, L. Sun, X. Lou, F. Yang, M. Feng, and J. Liu, "Chemical instability of graphene oxide following exposure to highly reactive radicals in advanced oxidation processes," *J. Colloid Interface Sci.*, vol. 507, pp. 51–58, Dec. 2017.

[17] Y. Tang, L. Dong, S. Mao, H. Gu, T. Malkoske, and B. Chen, "Enhanced photocatalytic removal of tetrabromobisphenol A by magnetic CoO@ graphene nanocomposites under visible-light irradiation," *ACS Appl. Energy Mater.*, vol. 1, no. 6, pp. 2698–2708, 2018.

[18] W. Khan, A. K. Singh, S. Naseem, S. Husain, M. Shoeb, and M. Nadeem, "Synthesis and magnetic dispersibility of magnetite decorated reduced graphene oxide," *Nano-Struct. Nano-Objects*, vol. 16, pp. 180–184, Oct. 2018.

[19] P. Raizada, A. Sudhaik, and P. Singh, "Photocatalytic water decontamination using graphene and ZnO coupled photocatalysts: A review," *Mater. Sci. Energy Technol.*, vol. 2, no. 3, pp. 509–525, 2019.

[20] R. Gusain, K. Gupta, P. Joshi, and O. P. Khatri, "Adsorptive removal and photocatalytic degradation of organic pollutants using metal oxides and their composites: A comprehensive review," *Adv. Colloid Interface Sci.*, vol. 272, Oct. 2019, Art. no. 102009.

[21] Y. Y. Kannangara, R. Wijesena, R. Rajapakse, and K. de Silva, "Heterogeneous photocatalytic degradation of toluene in static environment employing thin films of nitrogen-doped nano-titanium dioxide," *Int. Nano Lett.*, vol. 8, pp. 31–39, Apr. 2018.

[22] Y. Y. Kannangara, U. A. Rathnayake, and J.-K. Song, "Redox active multilayered Zn-pPDA MOFs as high-performance supercapacitor electrode material," *Electrochim. Acta*, vol. 297, pp. 145–154, Feb. 2019.

[23] C. Ma, K. Yang, L. Wang, and X. Wang, "Facile synthesis of reduced graphene oxide/Fe_3O_4 nanocomposite film," *J. Appl. Biomater. Funct. Mater.*, vol. 15, pp. e1–e6, Jun. 2017.

[24] A. K. Mishra and S. Ramaprabhu, "Magnetite decorated graphite nanoplatelets as cost effective CO_2 adsorbent," *J. Mater. Chem.*, vol. 21, no. 20, pp. 7467–7471, 2011.

[25] D. Shi, J. P. Cheng, F. Liu, and X. B. Zhang, "Controlling the size and size distribution of magnetite nanoparticles on carbon nanotubes," *J. Alloys Compounds*, vol. 502, no. 2, pp. 365–370, Jul. 2010.

[26] Y. Yoon, W. K. Park, T.-M. Hwang, D. H. Yoon, W. S. Yang, and J.-W. Kang, "Comparative evaluation of magnetite–graphene oxide and magnetite-reduced graphene oxide composite for As(III) and As(V) removal," *J. Hazardous Mater.*, vol. 304, pp. 196–204, Mar. 2016.

[27] D. Zhao, H. Zhu, C. Wu, S. Feng, A. Alsaedi, T. Hayat, and C. Chen, "Facile synthesis of magnetic Fe_3O_4/graphene composites for enhanced U(VI) sorption," *Appl. Surf. Sci.*, vol. 444, pp. 691–698, Jun. 2018.

[28] A. G. Roca, J. F. Marco, M. D. P. Morales, and C. J. Serna, "Effect of nature and particle size on properties of uniform magnetite and maghemite nanoparticles," *J. Phys. Chem. C*, vol. 111, no. 50, pp. 18577–18584, Dec. 2007.

[29] L. Nalbandian, E. Patrikiadou, V. Zaspalis, A. Patrikidou, E. Hatzidaki, and C. N. Papandreou, "Magnetic nanoparticles in medical diagnostic applications: Synthesis, characterization and proteins conjugation," *Current Nanosci.*, vol. 12, no. 4, pp. 455–468, 2016.

[30] W. Wu, C. Jiang, and V. A. Roy, "Recent progress in magnetic iron oxide-semiconductor composite nanomaterials as promising photocatalysts," *Nanoscale*, vol. 7, pp. 38–58, Oct. 2015.

[31] P. C. L. Muraro, S. R. Mortari, B. S. Vizzotto, G. Chuy, C. D. Santos, L. F. W. Brum, and W. L. da Silva, "Iron oxide nanocatalyst with titanium and silver nanoparticles: Synthesis, characterization and photocatalytic activity on the degradation of Rhodamine B dye," *Sci. Rep.*, vol. 10, pp. 1–9, Feb. 2020.

[32] Y. Y. Kannangara, U. A. Rathnayake, and J.-K. Song, "Hybrid supercapacitors based on metal organic frameworks using *p*-phenylenediamine building block," *Chem. Eng. J.*, vol. 361, pp. 1235–1244, Apr. 2019.

[33] G. Eda and M. Chhowalla, "Chemically derived graphene oxide: Towards large-area thin-film electronics and optoelectronics," *Adv. Mater.*, vol. 22, no. 22, pp. 2392–2415, 2010.

[34] F. Tuinstra and J. L. Koenig, "Raman spectrum of graphite," *J. Chem. Phys.*, vol. 53, no. 3, pp. 1126–1130, Aug. 1970.

[35] Y.-J. Lin and C.-T. Lee, "Surface analysis of $(NH_4)_2S_x$-treated InGaN using X-ray photoelectron spectroscopy," *J. Vac. Sci. Technol. B, Microelectron. Nanometer Struct. Process., Meas., Phenomena*, vol. 19, pp. 1734–1738, Sep. 2001.

[36] L. Li, P. Ma, S. Hussain, L. Jia, D. Lin, X. Yin, Y. Lin, Z. Cheng, and L. Wang, "FeS_2/carbon hybrids on carbon cloth: A highly efficient and stable counter electrode for dye-sensitized solar cells," *Sustain. Energy Fuels*, vol. 3, no. 7, pp. 1749–1756, 2019.

[37] Z. Hou, P. Yan, B. Sun, H. Elshekh, and B. Yan, "An excellent soft magnetic Fe/Fe_3O_4-FeSiAl composite with high permeability and low core loss," *Results Phys.*, vol. 14, Sep. 2019, Art. no. 102498.

[38] A. Rajan, M. Sharma, and N. K. Sahu, "Assessing magnetic and inductive thermal properties of various surfactants functionalised Fe_3O_4 nanoparticles for hyperthermia," *Sci. Rep.*, vol. 10, p. 15045, Sep. 2020.

[39] P. Lazar, F. Karlický, P. Jurecka, M. Kocman, E. Otyepková, K. Šafáová, and M. Otyepka, "Adsorption of small organic molecules on graphene," *J. Amer. Chem. Soc.*, vol. 135, no. 16, pp. 6372–6377, Apr. 2013.

[40] S. Phanichphant, A. Nakaruk, K. Chansaenpak, and D. Channei, "Evaluating the photocatalytic efficiency of the $BiVO_4$/rGO photocatalyst," *Sci. Rep.*, vol. 9, p. 16091, Nov. 2019.

[41] S. Mahich, Y. K. Saini, K. Aggarwal, A. Kumar, D. Kumar, and A. Singh, "Removal of methylene blue dye by metal free adsorption and photodegradation method using different reduction grades of graphene oxide," *RSC Adv.*, vol. 9, pp. 37686–37695, 2019.

[42] M. Nadimi, A. Z. Saravani, M. A. Aroon, and A. E. Pirbazari, "Photodegradation of methylene blue by a ternary magnetic TiO_2/Fe_3O_4/graphene oxide nanocomposite under visible light," *Mater. Chem. Phys.*, vol. 225, pp. 464–474, Mar. 2019.

[43] R. A. Mahmud, A. N. Shafawi, K. A. Ali, L. K. Putri, N. I. M. Rosli, and A. R. Mohamed, "Graphene nanoplatelets with low defect density as a synergetic adsorbent and electron sink for ZnO in the photocatalytic degradation of methylene blue under UV-vis irradiation," *Mater. Res. Bull.*, vol. 128, Aug. 2020, Art. no. 110876.

[44] M. Israr, J. Iqbal, A. Arshad, S. O. Aisida, and I. Ahmad, "A unique $ZnFe_2O_4$/graphene nanoplatelets nanocomposite for electrochemical energy storage and efficient visible light driven catalysis for the degradation of organic noxious in wastewater," *J. Phys. Chem. Solids*, vol. 140, May 2020, Art. no. 109333.

[45] U. G. Akpan and B. H. Hameed, "Parameters affecting the photocatalytic degradation of dyes using TiO_2-based photocatalysts: A review," *J. Hazardous Mater.*, vol. 170, nos. 2–3, pp. 520–529, Oct. 2009.

[46] S. Song, Y. Wang, H. Shen, J. Zhang, H. Mo, J. Xie, N. Zhou, and J. Shen, "Ultrasmall graphene oxide modified with Fe_3O_4 nanoparticles as a fenton-like agent for methylene blue degradation," *ACS Appl. Nano Mater.*, vol. 2, no. 11, pp. 7074–7084, Nov. 2019.

N. P. EDIRISINGHE received the B.Sc. degree in mineral resources and technology from Uva Wellassa University, in 2016. She was with the Sri Lanka Institute of Nanotechnology (SLINTEC), until 2019. Her research interests include water and waste water purification and nanomaterials.

YASUN Y. KANNANGARA received the Ph.D. degree in engineering from Sungkyunkwan University, South Korea, in 2020. Since 2020, he has been with the Sri Lanka Institute of Nanotechnology (SLINTEC), where he is currently a Senior Research Scientist-(Grade-III) and heading the SLINTEC Energy Research Group. His research interests include nanomaterials, nanocomposites graphene, and electrode materials for energy storage devices.

SHADEEPA KARUNARATHNE received the B.Sc. (Hons.) and M.Phil. degrees in physics from the University of Kelaniya, in 2011 and 2014, respectively. He is currently pursuing the Ph.D. degree with Bournemouth University. He was the Science Group Leader with the Sri Lanka Institute of Nanotechnology (SLINTEC). His research interests include metal air batteries, electrocatalysts, 2D materials, plasma technology, energy storage devices, advanced nanomaterials, and gas sensing.

S. A. L. SAMEERA received the B.Sc. degree from the University of Sri Jayewardenepura, in 2017, and the M.Sc. degree in analytical chemistry from the University of Colombo, Sri Lanka, in 2023. From 2018 to 2019, he was with the Graphene Research Group, Sri Lanka Institute of Nanotechnology (SLINTEC). His research interests include nanomaterials, analytical chemistry, and embedded systems.

K. R. KOSWATTAGE received the B.Sc. degree in physics from the University of Colombo, Sri Lanka, in 2004, and the M.Sc. and Ph.D. degrees in physics from Kobe University, Japan, in 2009 and 2012, respectively. From 2012 to 2016, he was an Assistant Professor with Chiba University, Japan. He is currently a Professor and the Dean of the Faculty of Technology, Sabaragamuwa University of Sri Lanka. He is also an Adjunct Professor (honorary position) with General Sir John Kothalawala Defence University. He recently received more than 350 million LKR (U.S. $1.1 million) from ADB/competitive research grant as a principal investigator and established center for nanodevices fabrication and characterizations. His research interests include the surface and interface analysis and characterization of some organic, inorganic, and biomaterials using synchrotron spectroscopies in VUV and soft x-ray regions.

H. C. S. PERERA received the B.Sc. degree in physics from the University of Peradeniya, Sri Lanka, in 2012, and the Ph.D. degree from the Queensland University of Technology (QUT), Australia, in 2016. Her Ph.D. degree was about studying the interaction between quantum dots and plasmon supported by plasmonic waveguides, including nanofabrication, characterization, and testing. From 2018 to 2022, she was a Senior Lecturer with the Department of Physics, University of Peradeniya. She is currently a Visiting Researcher Scholar (Faculty) with Khalifa University, United Arab Emirates. She closely collaborates with Dr. G. Das with Khalifa University. Her current research interests include synthesizing novel nanomaterials for environmental, industrial, and biological applications, such as wastewater treatment, self-cleaning materials, and drug delivery. In 2017, she received the Postdoctoral Research Scientist Award from NSF, Sri Lanka, to pursue research in infrared photodetection.

G. DAS has been an Associate Professor with Khalifa University, since 2019. Before joining Khalifa University, he was a Research/Staff Scientist with the King Abdullah University of Science and Technology (KAUST), Saudi Arabia, and the Team Leader with the Italian Institute of Technology, Genoa, Italy. He was involved in the fabrication and characterization of plasmonic devices for biomedical applications. He has vast experience with different techniques employed in micro and nanofabrication laboratories for fabricating different nanophotonics plasmonic devices. His H-index of 40, and his research works received more than 5900 citations. His research interest includes spectroscopy characterization to nanofabrication techniques for biomedical applications, including enhanced spectroscopy techniques, such as SERS, TERS, and near-field imaging.

M. M. M. G. P. G. MANTILAKA received the B.Sc. degree in applied sciences from the Faculty of Science, University of Peradeniya, in 2011, and the Ph.D. degree in nanotechnology from the Postgraduate Institute of Science (PGIS), University of Peradeniya, in collaboration with Loughborough University, U.K., in January 2015. He was a former Senior Scientist and a Coordinator/the Head of Advanced Materials with the Sri Lanka Institute of Nanotechnology (SLINTEC). He is currently the Director/CEO of the Institute of Materials Engineering and Technopreneurships (IMETechno) and a Scientist with the Center for Nanodevices Fabrication and Characterization, Faculty of Technology, Sabaragamuwa University of Sri Lanka. He is also a Visiting Senior Lecturer in nanotechnology with the Postgraduate Institute of Science (PGIS), the University of Peradeniya (former Senior Lecturer), the Rajarata University of Sri Lanka, and the South Eastern University of Sri Lanka. He is a Senior Scientist, a Senior Lecturer, and an Innovator in nanotechnology and materials science areas. He has commercialized research and development more than 50 innovative products under brands, including the ^{VIS}Viroshield antimicrobial solution range, Atlas antibacterial book, self-cleaning product range under ^{VIS}Lotus, fertilizer range, and fertilizer nutrients enhancers under the brand nHancer, and many mineral-based products, and MagGenome DNA Extraction kits. His research record includes 12 patents, 42 published papers in reputed international journals, two book chapters, about 100 conference papers, and five magazine/newspaper articles. He became the Most Outstanding Young Earth Scientist in Sri Lanka, in 2013, closely collaborates receiving P. G. Cooray Medal. He has also received several presidential awards and an NRC merit award for his international publications.

W. P. S. L. WIJESINGHE received the B.Sc. (Hons.) and Ph.D. degrees in nanotechnology and material science from the University of Peradeniya, in 2011 and 2015, respectively. Since 2017, he has been with the Sri Lanka Institute of Nanotechnology (SLINTEC), where he is currently a Senior Research Scientist II and leads the SLINTEC Mineral, and Advanced Material Research Group. His research interests include biomaterials, polymers, ceramics, nanocomposites graphene, gas sensing materials, and electrode materials for energy storage device.

• • •